Journal of the Brazilian Society of Mechanical Sciences and Engineering (2018) 40:213
https://doi.org/10.1007/s40430-018-1107-7

TECHNICAL PAPER

A study on mechanical behavior and wear performance of a metal–metal Co–30Cr biomedical alloy with different molybdenum addition and optimized using Taguchi experimental design

Amit Aherwar[1] · Amit Singh[2] · Amar Patnaik[1]

Received: 29 October 2016 / Accepted: 21 September 2017 / Published online: 27 March 2018

Abstract
Molybdenum-added biomedical alloy has been prepared using a high-temperature vertical vacuum casting technique with five (0, 1, 2, 3, and 4 wt%) diverse weight percentages. The density, microhardness, and sliding wear behavior of the fabricated alloys were studied, showing that the addition of molybdenum content in the metal–metal alloy (i.e., Co–30Cr) increases the density from 7.2 to 8.7 g/cc for 0–4 wt% of Mo, respectively. Similarly, the hardness of prepared biomedical alloy also increases from 653 to 720 HV on addition of 0–4 wt% Mo particulate, respectively. The hardness is investigated by the microhardness tester. The aim of this current research work is to optimized the sliding wear behavior of molybdenum-added Co–30Cr alloy for implant material by Taguchi experimental design technique at five different normal loads (5–25 N), sliding velocities (0.26–1.3 m/s), sliding distance (500–2500 m), and reinforcement, i.e., Mo (0–4 wt%) respectively. To obtain the optimum wear response of prepared biomedical alloy added with Mo contents, the Taguchi L_{25} orthogonal array was implemented. The wear test is performed on a pin-on-disc tribometer against a hardened alloy steel (EN-31) disc under different operating conditions at room temperature. Afterwards, field-emission scanning electron microscopy and atomic force microscopy were utilized to analyze the microstructure, contour of wear mechanism, and 3D surface topography of samples after test run.

Keywords Molybdenum · Mechanical · Sliding wear · Design of experiment · FESEM/EDAX

1 Introduction

The real challenges faced by a researcher in the field of biomaterial are the selection of apposite constituents with accurate weight percentage and design of formulation for optimized physical, mechanical, and wear properties. Metallic biomaterials are the prime biomaterials utilized for joint replacement and are becoming increasingly important. The metallic biomaterials utilized for orthopedic applications can be categorized as stainless steel, cobalt–chrome alloys, and titanium and titanium alloys. These metallic biomaterials have several properties for example good thermal conductivity, high fracture toughness, hardness, high strength, corrosion resistance, and good biocompatibility, which make them a magnificent option for joint replacement [1]. Currently, Cobalt-based alloys are among the unharmed metallic biomaterials for hip implants, owing to their superior corrosion properties, mechanical strength, and biocompatibility [2–5]. The main trait of Co-based alloys is its corrosion resistance in chloride milieus, which is due to alloying additions and the formation of the chromium oxide Cr_2O_3 passive layer [3]. Cobalt–chrome alloy is much attuned to the human body. As a result of this, it is commonly used as implants and fixations. In contrast with other materials used in orthopedic fixations, cobalt chrome alloys have a superior biocompatibility than stainless steel but lesser than titanium. The fabrication of cobalt-based orthopedic metal alloys can be cast, wrought, and forged [4], but, nowadays, cobalt-based materials with improved properties have been fabricated by means of powder metallurgy [5, 6] and additive

Technical Editor: Francisco Ricardo Cunha.

✉ Amit Aherwar
amit.aherwar05@gmail.com

[1] Mechanical Engineering Department, Madhav Institute of Technology and Science, Gwalior 474005, India

[2] Mechanical Engineering Department, Malaviya National Institute of Technology, Jaipur 302017, India

manufacturing [7] also. Fuzeng et al. [8] fabricated the nickel and carbides free Co–28Cr–6Mo alloy using warm pressing technique and investigated the mechanical and tribological properties for biomedical applications. The microstructure of cobalt-based alloys comprises of a cobalt-rich solid solution matrix including carbides (i.e., Cr_7C_3, and $M_{23}C_6$) within the grains and at grain boundaries, where chromium, tungsten, tantalum, silicon, zirconium, nickel, and cobalt may be present in a single carbide particle [3, 9]. Commonly, wear properties are influenced by the size of the carbide phases and volume fraction. The coarser carbide particles result in more weight loss [9]. Typically, molybdenum produces a finer grain which results in improved mechanical properties and provides solid solution strengthening and good localized corrosion resistance [10, 11].

The main reason of failure of implant material for hip component is through aseptic loosening owing to wear that occurs between the bearing surfaces. Hence, wear is a prime factor to be considered. It has been shown that restricting the wear factor can play a significant role in the longevity viability of the implant material [11, 12]. The latest generation of metal-on-metal hip prosthesis has a new target of minimizing the amount of nanodebris produced by wear, which has been related to metal ion release in the human body [13]. One more problem which has been addressed by numerous researchers is the selection of an adequate lubricant to imitate the in vivo conditions undertaken by the prosthetic joint materials [14]. From the literature cited above, it is clear that countless studies have been conducted using the addition of molybdenum with different wt% which was mixed with different metal–metal alloys for distinct applications in a specific range and investigated their mechanical properties and wear performance, but none of the author has optimized the sliding wear loss of femoral head biomaterial for hip joint component so far.

Therefore, in the present research work, a series of metal–metal cobalt–chromium (i.e., Co–30Cr)—based alloy added with different weight percentages (0, 1, 2, 3, and 4 wt%) of molybdenum content were prepared using high-temperature induction furnace and then evaluated for physical, mechanical, and wear properties for orthopedic applications. An economic and feasible experimental plan based on Taguchi's parametric design has been utilized to optimize the wear loss and to study the influence of various parameters. After investigated and optimized the wear performance experimentally, SEM and AFM were utilized to examine the compositional analysis, microstructures, and morphology of the fabricated alloys.

2 Experimental details

2.1 Specimen preparation

The fabrication of molybdenum (less than 44 microns) added Co–30Cr metal alloy plates was performed on a high-temperature vacuum casting induction furnace, as shown in Fig. 1. This furnace consists of two major sections, i.e., one heating section that consisting of bottom pouring cylindrical graphite crucible attached to the vertical graphite plunger (8 mm in diameter) and around the graphite crucible heating coils are wound. At the top of the heating section, an infrared temperature measuring sensor is attached with magnifying glass to measure the temperature of inside the crucible. The periphery of the upper heating section of one additional layer is fixed where cooling water is consistently circulated to protect the heating section. The second major section is the casting section where rectangular graphite mold is placed. Once the molten material is melted, the plunger is opened and the molten material will pour vertically into the rectangular graphite mold. Prior to the fabrication process was started out, respective weight percentages of all three proposed materials (see in Table 1) were pre-heated first in another furnace up to 200 °C; and after pre-heating, the proposed materials according to formulations were heated in the cylindrical graphite crucible attached to the high-temperature vacuum casting induction furnace. Once the base material attained above its liquid temperature, i.e., 1800 °C, the molybdenum powder (See Fig. 2) was in pre-heated form poured in the molten metal alloy slowly according to required quantity in different wt% for 6–8 min. When the mixture of molybdenum and base material attained the plunger which was affixed to the hood section (see Fig. 1) of the furnace was opened and the molybdenum-added molten metal was dropped vertically downward into the rectangular graphite mold of size of $120 \times 65 \times 10$ mm^3 and then cool it by quench medium for 30 min. In this analysis, the rotational speed is maintained around 200 rpm for uniform mixing of molybdenum according to the formulation with the base materials. After casting, the rectangular mold is removed from the vacuum chamber and the samples were then sized as per the sample size; and the surface is ground and polished by semi automatic Buehler MetaServ 250 polisher/grinder, and then, samples were cleaned in ethanol with an ultrasonic cleaner and dried with a commercially available blower. For the sliding wear analysis, five groups of M-0, M-1, M-2, M-3, and M-4 (0–4 wt%) specimens were fabricated.

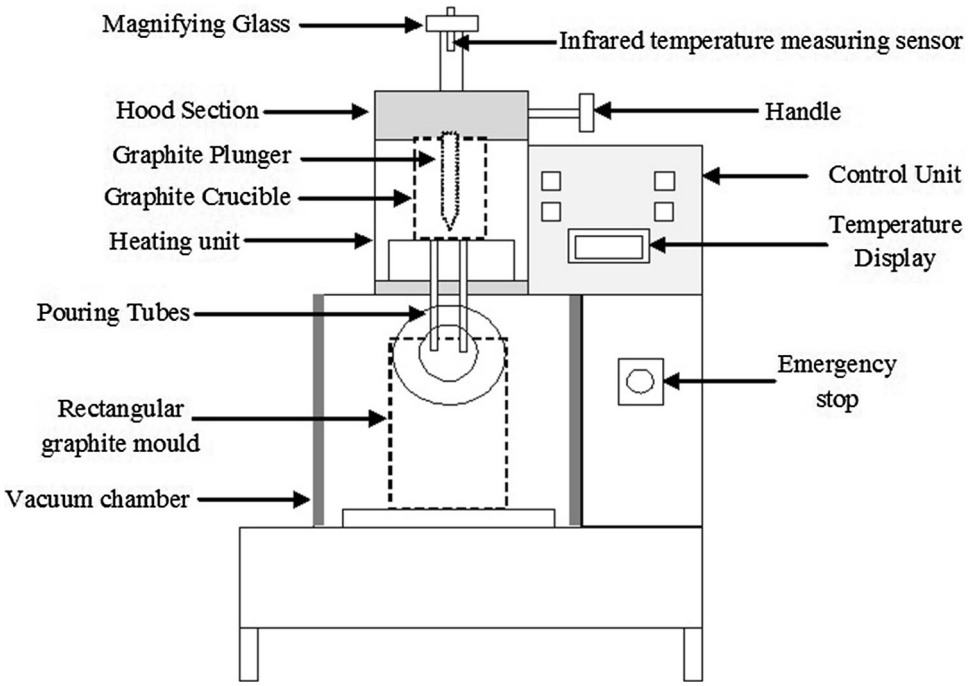

Fig. 1 Schematic diagram of high temperature vertical vacuum casting machine

Table 1 Chemical composition (wt%) and designation of samples (in weight percentage)

Material designation	Composition
M-0	Co balancing, 30% Cr, 0% Mo
M-1	Co balancing, 30% Cr, 1% Mo
M-2	Co balancing, 30% Cr, 2% Mo
M-3	Co balancing, 30% Cr, 3% Mo
M-4	Co balancing, 30% Cr, 4% Mo

2.2 Test of density and microhardness

Microhardness is analyzed over the USL Vickers microhardness testing machine having a square-based pyramidal (Angle 136° between opposite faces) diamond indenter by applying a load of 0.5 N for 15 s. All measurements were carried out as per ASTM E-92 standard. The microhardness is measured at six different locations and the mean was considered in this study. The density of the said alloys is obtained by the Archimedean principle by weighing the sample in air and then in water. For evaluation of density and hardness, five specimens are tested and mean values are reported.

2.3 Wear tests

A pin-on-disc tribometer confirming to ASTM G 99 [15] was utilized for carried out the tribo-performance of fabricated alloys supplied by DUCOM, Bangalore, India. The tribometer runs under stationary conditions with constant applied normal forces of up to 60 N and at constant rotational speeds of up to 2000 rpm. A load cell is utilized to evaluate the tangential force acting on the pin. The tribometer has a disc works as a counter body made up of hardened alloy steel (EN-31) with 60–70 Rockwell hardness (HRC) and surface roughness of 1.6 μm. During the test, the specimen (Pin) held stationary and the disc is rotated (see Fig. 3a) and the load is applied through a lever mechanism. Each sample, as shown in Fig. 3b, was tested using pin shaped with a 10 mm in length, 10 mm in width, and height of 20 mm. Two different steady-state conditions were applied with varying each of the parameters such as a normal load (5, 15, and 25 N) and sliding velocity (0.26, 0.78, and 1.3 m/s), by keeping other parameters constant. All experiments were performed 50 mm diameter of wear track. Each experiment run was repeated thrice and the average value was reported for more accuracy. After each experimental run, each sample is cleaned with cotton dipped in acetone and dried with a hot-air blower for 2 min. Thereafter, a precision electronic balance with accuracy ± 0.1 mg is utilized to find the material loss. Finally, the volumetric wear loss (mm^3) is computed as follows:

$$\text{Volumetric wear loss} = \frac{\Delta\omega}{\rho}, \tag{1}$$

where $\Delta\omega$ is mass loss of fabricated alloys during test (g) and ρ is the measured density of the fabricated samples (g/mm^3).

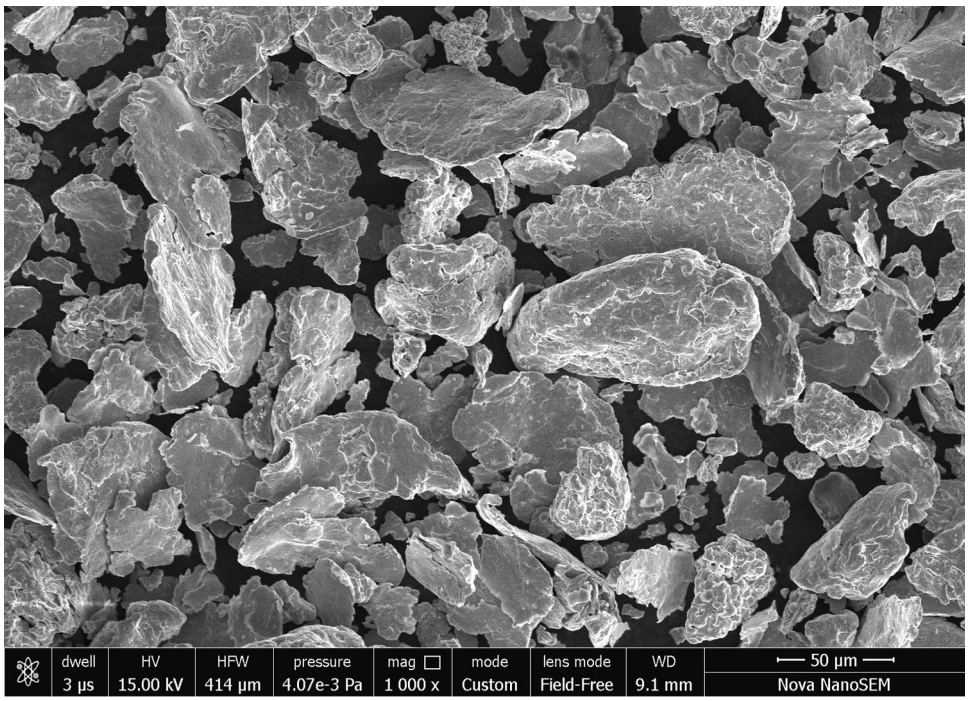

Fig. 2 SEM micrograph of Molybdenum powder

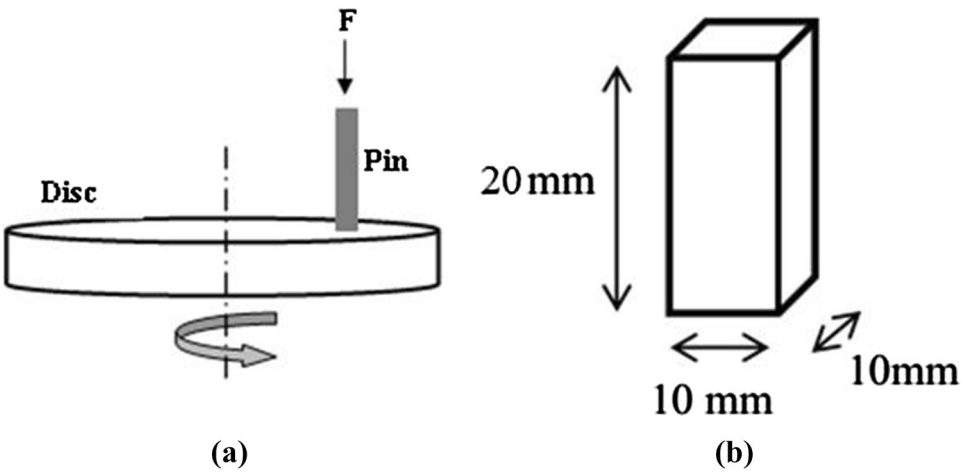

Fig. 3 **a** Arrangement of disc and pin; **b** pin sample

2.4 Taguchi experimental design

Taguchi design of experiments is a powerful analytical approach for exploring the influence of control factors on output performance. It is commonly adopted approach for optimizing design parameters because of its simple, efficient, and systematic. This experimental procedure has been used prior to study on the sliding wear response of hybrid composites using Taguchi experimental design by Aherwar et al. [16] and Patnaik et al. [17]. This technique basically reduces the number of experimental runs with no significant data loss and is an effectual method to solve the complex structure of the problem. In this study, the lower-is-better (LB) characteristics approach was applied as performance characteristics for the analysis of sliding wear of the fabricated biomedical alloys. For this, four factors, i.e., normal load, sliding velocity, sliding distance, and filler (i.e., Mo) contents were considered, as shown in

Table 2 Levels of the variables used in the experiment

Control factor	Level					Units
	I	II	III	IV	V	
A: Normal load	5	10	15	20	25	N
B: Sliding velocity	0.26	0.52	0.78	1.04	1.30	m/s
C: Sliding distance	500	1000	1500	2000	2500	m
D: Filler content	0	1	2	3	4	wt%

Table 2, in this present study; and a Taguchi L_{25} (5^6) orthogonal array design was employed for one response, i.e., sliding wear. The S/N ratio analysis with lower-is-better characteristics can be expressed as follows [18]:

$$(\eta) = -10\log\left[\frac{1}{n}\sum_{i=1}^{n} y_i^2\right], \quad (2)$$

where n is the number of runs and y_i is the experimental value of the ith run.

2.5 Microstructure characterization and surface morphology

The prepared samples were first electrolytically etched with 100 ml ethanol and 20 ml 1.0 M HCl mixed with copper(II) chloride ($CuCl_2$) for 10 s and then FESEM attached with EDAX (FEI NOVA NANO 450) was utilized to analyze their microstructure, diverse phases, and wear mechanisms originated by the wear test. The molybdenum compounds in the entire samples were examined using Panalytical X Pert Pro X-ray diffractometer (XRD) with monochromatic CuKα radiation over $20° \leq 2\theta \leq 100$. X'Pert High Score software and the PCPDF data bank were used to carry out the pattern analysis of the samples. Atomic force microscopy (AFM) surface examination was also carried out to analyze the surface contour on samples after test runs. All the worn surface profiles were recorded at ambient temperature (25 °C and 30% relative humidity).

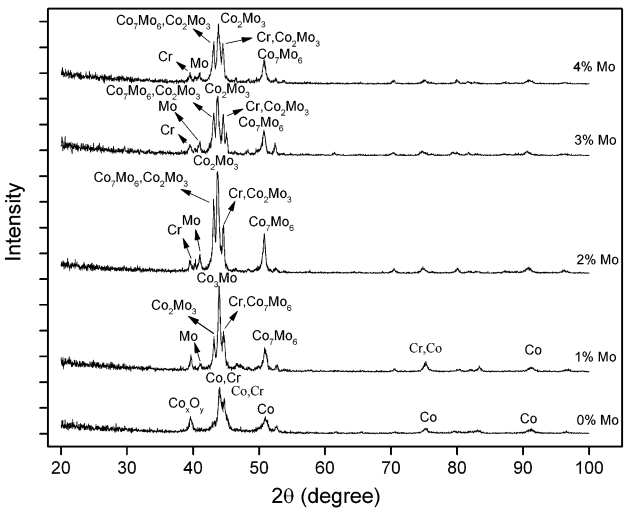

Fig. 4 XRD patterns of Mo free and Mo added Co–30Cr alloys with different wt%

3 Results and discussion

The XRD diffractograms with a comparison for each sample are presented in Fig. 4. It can be seen that the microstructure of 0 wt% Mo consists of a Co matrix with Cr regions. It is clear that the Co, in alliance with oxide forms Co_xO_y in the microstructure. The necessary oxides could have arrived from two sources: from Co or from the atmosphere for the period of mixing. In addition, the hexagonal close-packed (HCP) Co structure has been formed for the reason that of the martensitic transformation [19]. No carbides (i.e. M_7C_3) are observed in the microstructure, which corresponds well with the XRD peaks identified in 0–4 wt.% Mo content. On the other hand, in all the samples, the FCC (111) cobalt base α matrix (d = 2.04 Å, $a = b = c$ = 3.545 Å), bcc (110) Cr (d = 2.039 Å, $a = b = c$ = 2.884 Å), BCC (110) Mo (d = 2.225 Å, $a = b = c$ = 3.147 Å), and HCP (201) Co_3-Mo (d = 1.953 Å, $a = b$ = 5.125 Å, c = 4.113 Å) were identified. An additional rhombohedral Co_7Mo_6 (116) phase (d = 2.08 Å), Co_7Mo_6 (027) phase (d = 1.796 Å, $a = b$ = 4.762 Å, and c = 25.617 Å) and a tetragonal Co_2Mo_3 (411) phase (d = 2.031 Å, $a = b$ = 9.229 and c = 4.827 Å) were identified. The XRD patterns obtained in this study are similar to the previous studies that Cr-rich carbides transform from M_7C_3 to $M_{23}C_6$ in a different cobalt-based satellite alloy (i.e. Co–Cr–W–C) [20–25]. The SEM image of the microstructure of Mo-free and Mo-added metal alloys (i.e., M0, M1, M2, M3, and M4) is shown in Fig. 5a–e. It can be seen that the cobalt-based solid solution is in light gray, chromium is in dark gray, and, in different shades of black, the molybdenum contents.

3.1 Density and hardness test

The effect of molybdenum on the density and hardness is shown in Fig. 6. It was observed that the molybdenum content has caused a distinct transition in density and hardness and subsequently improved its both significantly. This improvement in density may be attributed to the addition of particulate (Mo) with their increased bonding and better intermixing in the matrix causing an increase in the bulk entanglement density. The densities obtained with the addition of molybdenum particulate (0–4 wt% Mo) have near about as per ASTM F75 [23]. Furthermore, with reinforcement, the micropacking of the particulate in the matrix improves the mechanical integrity resulting in increased hardness and reaches a maximum value of 720 HV at M-4 metal alloy. A similar trend was reported by Nwambu et al. [24] for the hardness of Aluminium—12.5 Si alloys. The author investigated the influence of cobalt and molybdenum on the microstructure and

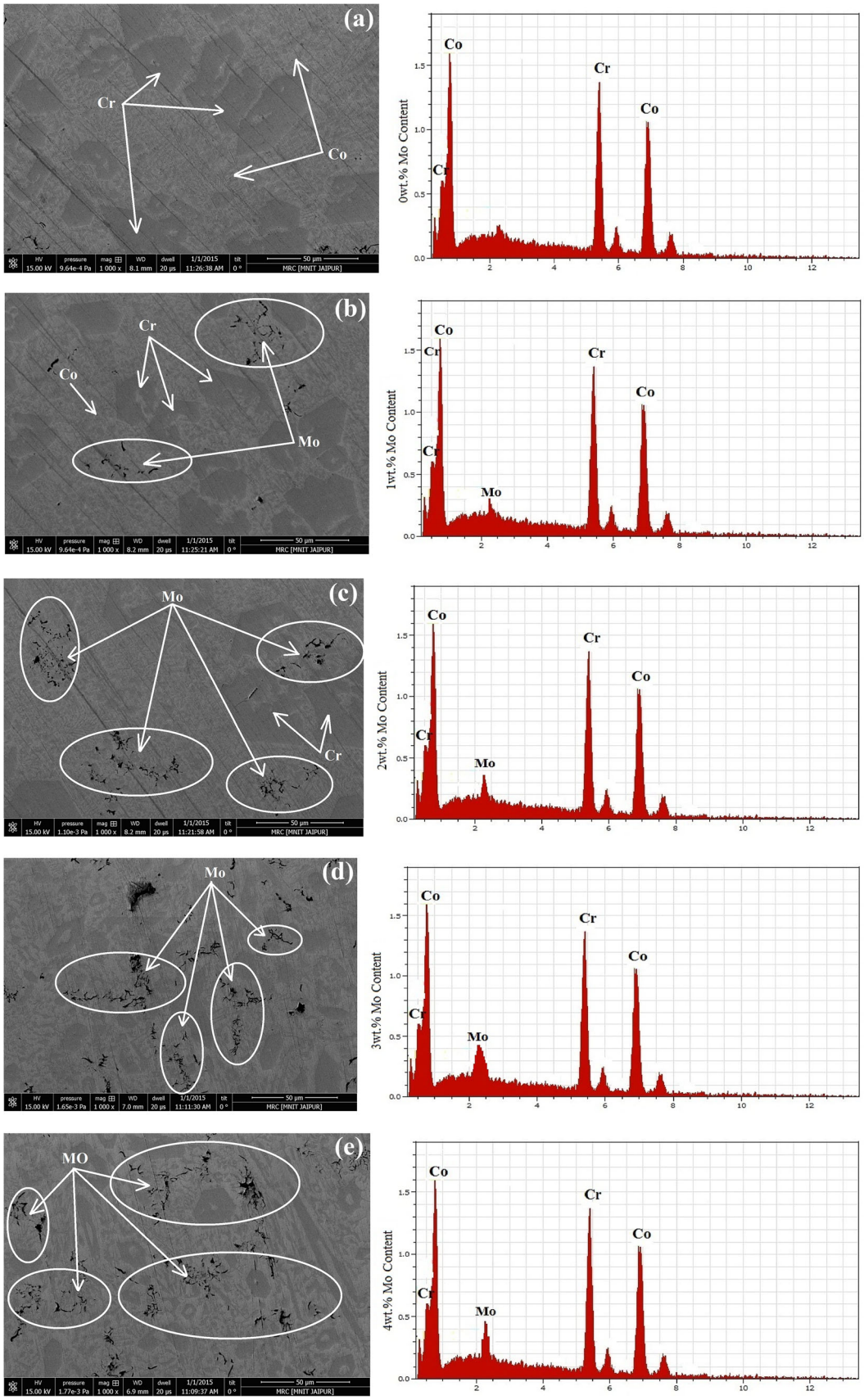
(a)
Cr
Co
0wt.% Mo Content
Co
Cr
Co
Cr
(b)
Cr
Co
Mo
1wt.% Mo Content
Co
Cr
Cr
Co
Cr
Mo
(c)
Mo
Cr
2wt.% Mo Content
Co
Cr
Co
Cr
Mo
(d)
Mo
3wt.% Mo Content
Co
Cr
Co
Cr
Mo
(e)
MO
4wt.% Mo Content
Co
Cr
Co
Cr
Mo

◀**Fig. 5** SEM micrographs and corresponding EDS results of samples with different wt% molybdenum **a** 0 wt% Mo, **b** 1 wt% Mo, **c** 2 wt% Mo, **d** 3 wt% Mo, **e** 4 wt% Mo

mechanical properties of the Al—12.5 Si alloy. Shin et al. [25] also reported the effect of molybdenum on Stellite 6 hard facing alloys and showed that the hardness is increased as the wt% Mo becomes higher.

3.2 Steady-state volumetric wear loss

3.2.1 Effect of sliding velocity on volumetric wear loss of molybdenum-added Co–30Cr alloy

The sliding wear analyses in a steady-state condition as shown in Fig. 7a are conducted by varying one parameter at-a-time, i.e., sliding velocity and rest all other operating parameters such as: normal load (15 N) and sliding distance (1500 m) remained constant at room temperature. It is clearly shown in Fig. 7a, the volumetric wear loss gradually increased with the increased in sliding velocity irrespective of molybdenum content. The volumetric wear loss attained maximum in 3 wt% Mo-added metal alloy (i.e., Co–30Cr–3Mo) at 1.3 m/s is sliding velocity and minimum in 4 wt% Mo-added metal alloy (i.e., Co–30Cr–4Mo) under the same operating condition. The improved wear resistant may be attributed to strong interface bonding between matrix material and molybdenum contents that intact material against wear out phenomenon. A similar trend obtained using plasma transferred arc process for nickel-based alloy coating reported by Hou et al. [26] and showed that the wear loss decreases as the molybdenum content in nickel-based alloy increased.

Figure 7b shows the effect of molybdenum on the friction coefficient with sliding velocity. At the primary epoch of rubbing, friction is low and the factors accounting for this low friction are due to the attendance of a layer of foreign material on the disc surface. This layer generally constitutes; moisture; oxide of metals; deposited lubricating material, etc. After an initial rubbing, the upper layer separates out and the fresh surfaces directly come in contact with each other, which increase the bonding force between them. A similar finding was reported by Savarimuthu et al. [27] for sliding wear behavior of tungsten carbide thermal spray coatings for replacement of chromium electroplate in aircraft applications. The 4 wt% Mo-added alloy displays least effect on the variation of friction coefficient with sliding velocity. The mean steady-state values of the friction coefficient with respect to sliding velocity tested at 15 N load are illustrated in Fig. 7b for the addition of Mo content metal alloys. It is clearly seen in Fig. 7b that, at the lowest sliding velocity (0.26 m/s) friction coefficient of almost all the combination of alloys, are low after which it increases and then decreases parallel to increase in the sliding velocity up to 0.785 m/s.

3.2.2 Effect of normal load on volumetric wear loss of molybdenum-added Co–30Cr alloy

Figure 8a shows the influence of molybdenum on volumetric wear loss with varying normal load (5–25 N) at a constant sliding velocity (0.785 m/s) and sliding distance (1500 m). As shown in Fig. 8a, volumetric wear loss

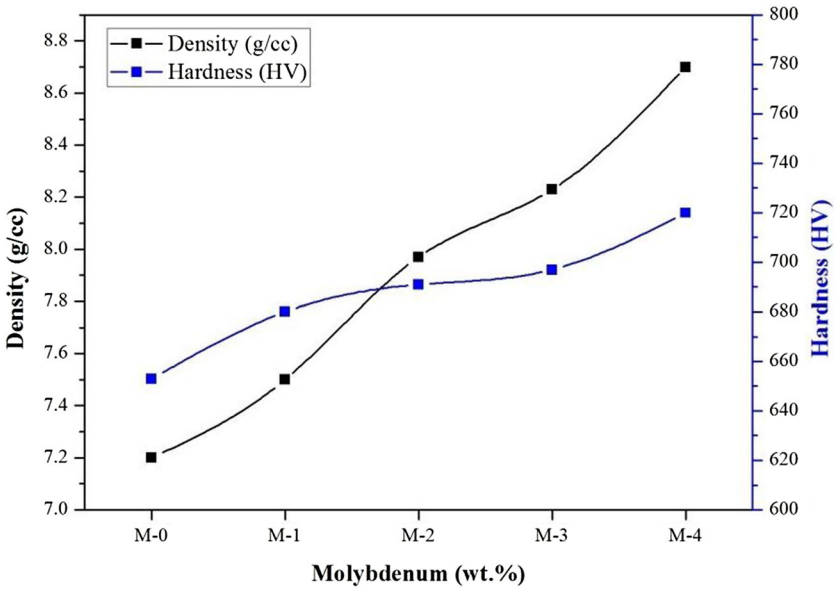

Fig. 6 Variation of density and hardness of molybdenum added alloys

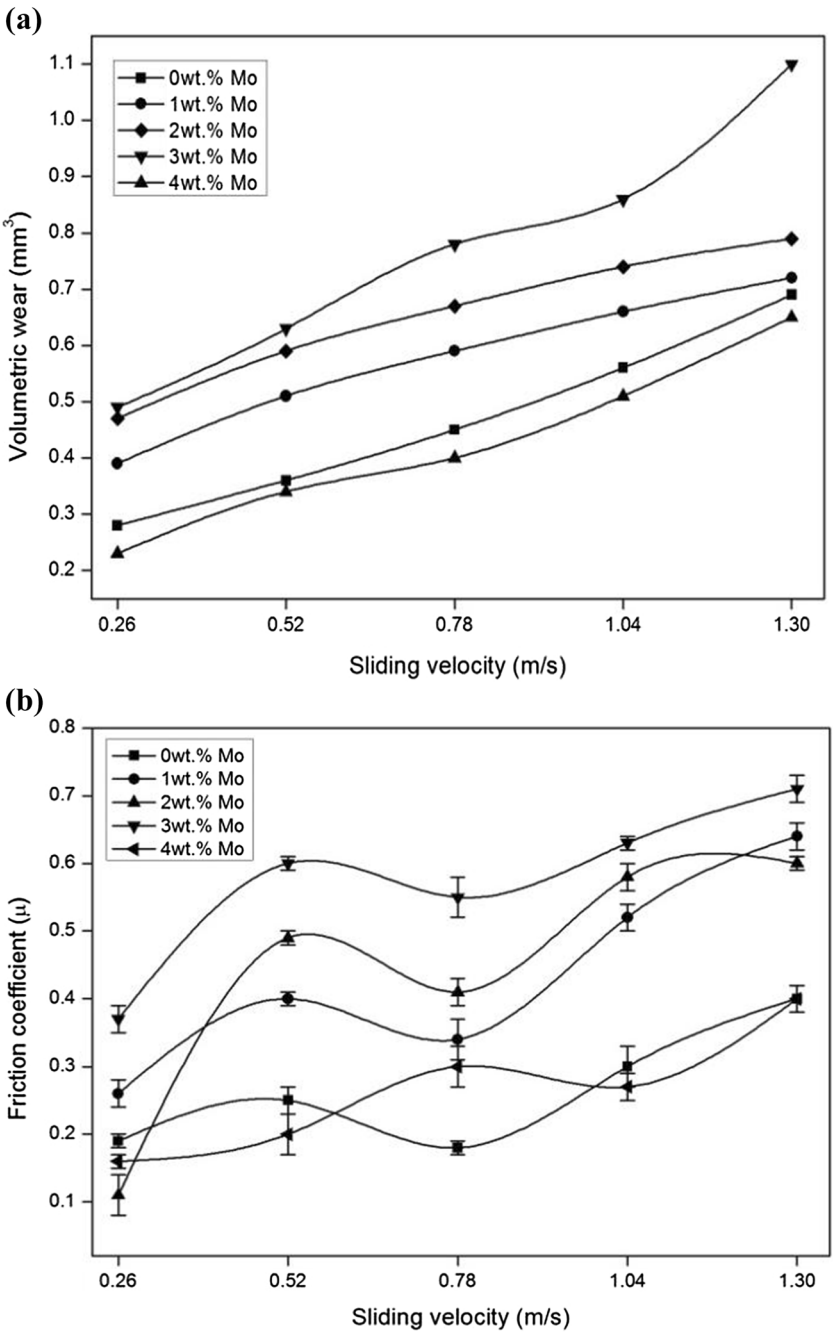

Fig. 7 **a** Variation of volumetric wear loss with sliding velocity for Co–30Cr alloy with different wt% of Mo (load: 15 N and sliding distance 1500 m). **b** Variation of friction coefficient with sliding velocity for Co–30Cr alloy with different wt% of Mo (load: 15 N and sliding distance 1500 m)

steadily increases if the normal load increased from 5 to 25 N. As the normal load is enhanced on the pin, the actual contact area would enhance to the nominal contact area, consequently that increase the frictional force between two contacting surfaces. This implies that the shear force and frictional thrust are enhanced with the increase of applied load and this accelerates the volumetric wear. Out of all weight percentages, M-3 alloy (i.e. Co–30Cr–3Mo) exhibits maximum wear loss, i.e., 0.56 mm^3, whereas M-4 alloy (i.e., Co–30Cr–3Mo) has maximum wear resistance than the others. The presence of molybdenum in the Co–30Cr alloy forms a good-quality transfer film that adheres nicely to the rubbing surfaces, thereby reducing wear performance. In this study, the material used for pin and counter disc is both different and the result observed of wear loss is similar to the earlier studies [28–30]. Some authors used the same material of pin and disc instead of EN31 steel. Firkins et al. [29] used CoCr alloy for both the pin and disc material; and found that the wear behavior is likely similar to our study. Doni et al. [30] compared the dry sliding wear behavior under 1 N normal load of hot-pressed CoCrMo implant material with commercially cast

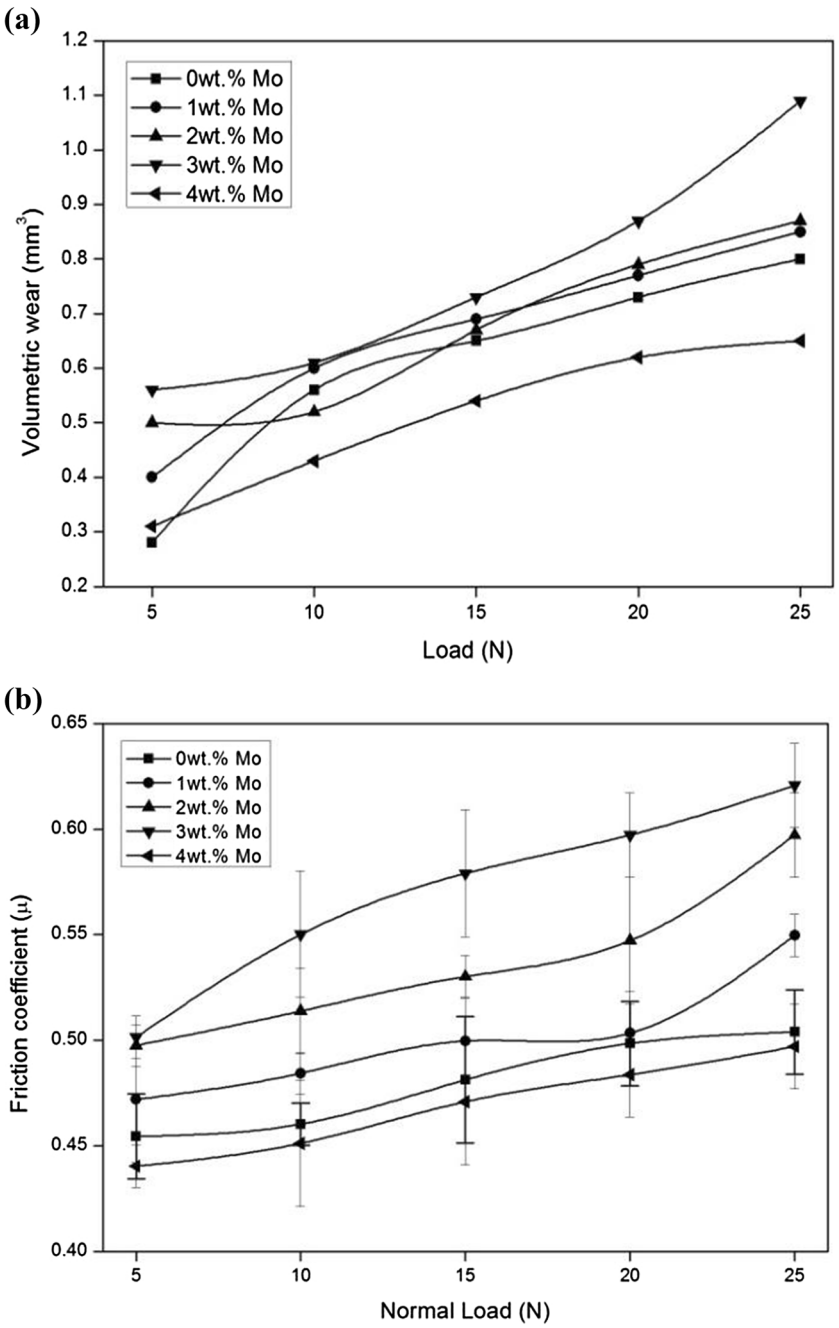

Fig. 8 **a** Variation of volumetric wear loss with normal load for Co–30Cr alloy with different wt% of Mo (sliding velocity: 0.785 m/s and sliding distance 1500 m). **b** Variation of friction coefficient with normal load for Co–30Cr alloy with different wt% of Mo (sliding velocity: 0.785 m/s and sliding distance 1500 m)

CoCrMo and Ti6Al4V implant materials, and found that the wear rate of Ti6Al4V alloy was 14 and 47 times higher than the cast and hot-pressed CoCrMo samples, respectively.

The effect of molybdenum on the friction coefficient with varying normal load (5–25 N) under the steady-state condition is depicted in Fig. 8b. It is observed that molybdenum contents have caused a distinct transition in terms of their performance. As shown in Fig. 8b, friction coefficient remains higher for 3 wt% molybdenum-added metal alloy at 25 N normal load. However, 4 wt% molybdenum mixed Co–30Cr alloy material has a little effect on the variation of friction coefficient of implant materials. The friction coefficient undergoes a substantial drop with the inclusion of 4 wt% Mo content in the metal–metal Co–30Cr biomedical alloy. This may be understandably been attributed to the presence of molybdenum, which maintains a transfer film between the contact surfaces. This film makes the contact area slippage of the two mating surfaces past each other at ease resulting in reduced friction coefficient [31].

3.3 Taguchi experimental analysis

Table 3 shows the volumetric wear loss and friction coefficient of molybdenum-free and molybdenum-added metal alloys and their respective S/N ratio values. The overall mean for the S/N ratio of the wear loss and friction coefficient are found to be − 9.777 and 6.670 dB, respectively. The values attained using popular MINITAB 16 software, specially used for DOE applications. Maximum signal-to-noise ratio corresponds to a minimum wear loss/friction coefficient and minimum signal-to-noise ratio corresponds to a maximum wear loss/friction coefficient. Figure 9a, b shows the effect of the control factors on wear volume and friction coefficient graphically. The distinct responses of signal-to-noise ratio for wear loss between the highest and lowest are also represented in Table 4. The normal load and sliding distance have the highest delta values, 12.159 and 10.892, respectively. Based on the Taguchi theory, higher the delta value of S/N ratio will have a more significant effect on wear loss. Hence, it can say that increasing the normal load will increase the wear loss significantly and also the sliding distance. From Fig. 9a, it is clearly seen that wear loss reduces (max. signal-to-noise ratio) with the increase in normal load at level-4 (at 20 N), sliding velocity at level-1 (at 0.26 m/s), sliding distance at level-5 (at 2500 m), and filler content at level-5 (at 4 wt%), respectively. Similarly, Table 4b and Fig. 9b show the S/N ratio responses for friction coefficient. It is clearly seen that the normal load and filler content have the highest delta values, 7.148 and 4.513, respectively. From Fig. 9b, it is seen that the friction coefficient reduces (max. signal-to-noise ratio) with the increase in normal load at level-1 (at 5 N), sliding velocity at level-2 (at 0.523 m/s), sliding distance at level-4 (at 2000 m), and filler content at level-5 (at 4 wt%), respectively. From this analysis, it concluded that the optimum factor combination of A_4, B_1, C_5, and D_5 gives minimum wear loss and factor combination of A_1, B_2, C_4, and D_5 gives a minimum friction coefficient for the fabricated biomedical metal alloys.

Table 3 Experimental design using L_{25} orthogonal array

Runs	A Load (N)	B Sliding velocity (m/s)	C Sliding distance (m)	D Filler content (wt%)	Wear volume (mm^3)	S/N ratio (db)	Friction coefficient (db)	S/N ratio (db)
1	5	0.26	500	0	7.2222	− 17.173	0.297	10.532
2	5	0.523	1000	1	9.5524	− 19.602	0.176	15.072
3	5	0.785	1500	2	7.3059	− 17.273	0.455	6.839
4	5	1.04	2000	3	6.0753	− 15.671	0.458	6.791
5	5	1.3	2500	4	2.2069	− 6.876	0.170	15.370
6	10	0.26	1000	2	9.0376	− 19.121	0.471	6.545
7	10	0.523	1500	3	3.2402	− 10.211	0.238	12.481
8	10	0.785	2000	4	2.1494	− 6.646	0.203	13.852
9	10	1.04	2500	0	3.1111	− 9.858	0.431	7.304
10	10	1.3	500	1	8.3333	− 18.416	0.350	9.108
11	15	0.26	1500	4	1.4541	− 3.252	0.463	6.679
12	15	0.523	2000	0	4.4753	− 13.016	0.466	6.634
13	15	0.785	2500	1	1.7067	− 4.643	0.731	2.722
14	15	1.04	500	2	6.6918	− 16.511	0.730	2.734
15	15	1.3	1000	3	1.6201	− 4.191	0.855	1.362
16	20	0.26	2000	1	0.3333	9.542	0.347	9.185
17	20	0.523	2500	2	1.6524	− 4.363	0.702	3.070
18	20	0.785	500	3	4.8603	− 13.733	0.888	1.032
19	20	1.04	1000	4	1.5747	− 3.944	0.753	2.469
20	20	1.3	1500	0	1.4630	− 3.305	0.696	3.151
21	25	0.26	2500	3	1.4977	− 3.508	0.787	2.086
22	25	0.523	500	4	7.8276	− 17.873	0.403	7.894
23	25	0.785	1000	0	2.8889	− 9.215	0.771	2.259
24	25	1.04	1500	1	2.6637	− 8.510	0.505	5.940
25	25	1.3	2000	2	2.2509	− 7.047	0.523	5.636

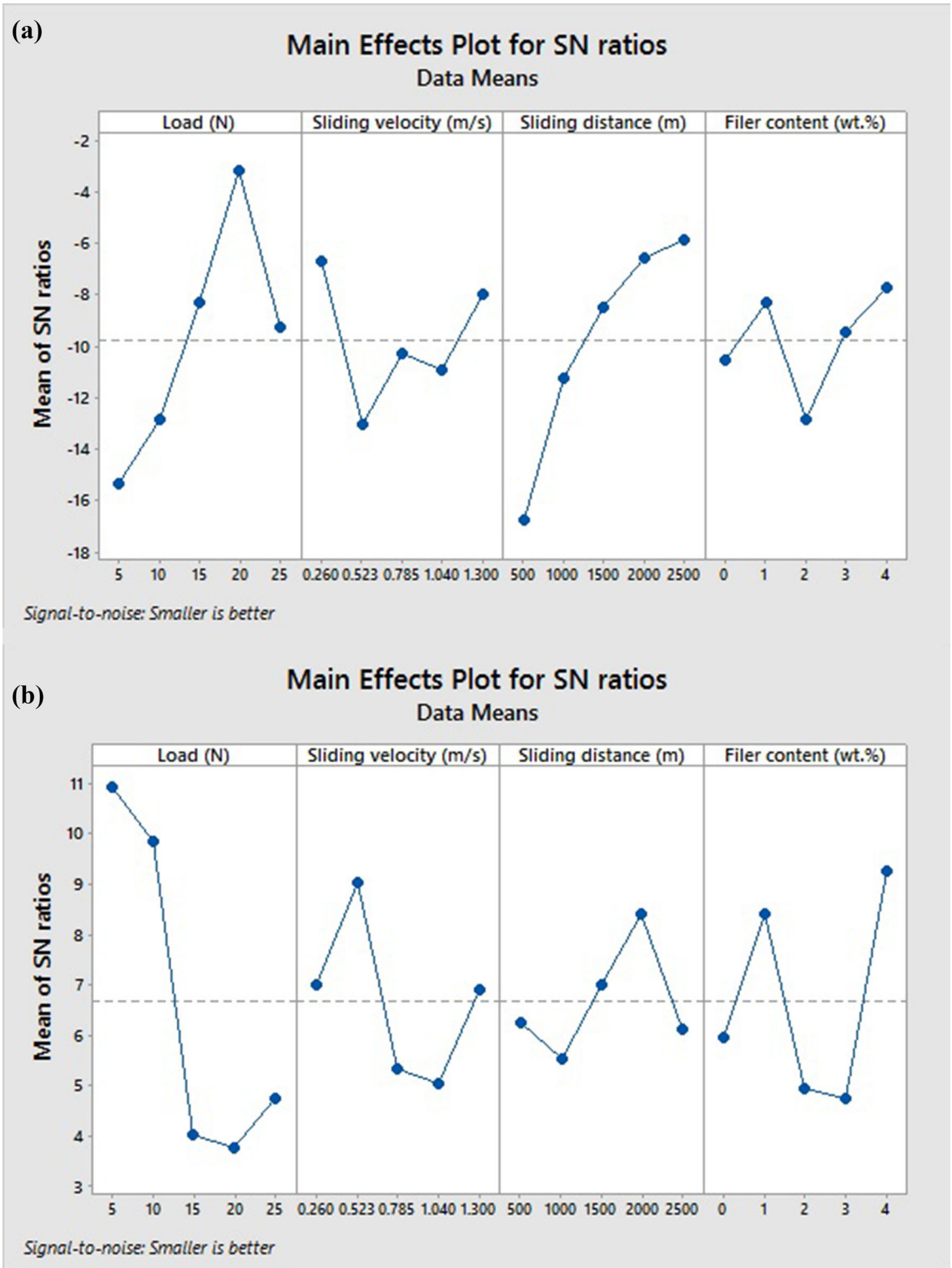

Fig. 9 **a** Effect of control factors on volumetric wear loss for Mo added Co–30Cr alloys. **b** Effect of control factors on friction coefficient for Mo added Co–30Cr alloys

Table 4 Signal-to-noise ratio for (a) wear loss, (b) friction coefficient

Level	A (Normal load)	B (Sliding velocity)	C (Sliding distance)	D (Filler content)
(a) Wear loss				
1	− 15.319	− 6.702	− 16.741	− 10.514
2	− 12.851	− 13.013	− 11.215	− 8.326
3	− 8.323	− 10.302	− 8.510	− 12.863
4	− 3.160	− 10.899	− 6.568	− 9.463
5	− 9.231	− 7.967	− 5.850	− 7.718
Delta	12.159	6.311	10.892	5.145
Rank	1	3	2	4
(b) Friction coefficient				
1	10.930	7.009	6.265	5.979
2	9.857	9.032	5.543	8.412
3	4.027	5.340	7.016	4.963
4	3.782	5.045	8.418	4.745
5	4.759	6.930	6.115	9.257
Delta	7.148	3.987	2.875	4.513
Rank	1	3	4	2

3.4 Surface morphology of worn samples in steady-state condition

The worn surface morphology of molybdenum-added Co–30Cr metal alloy was examined by scanning electron microscope. These micrographs have taken after 30 min of the test duration. The wear mechanism for molybdenum-free (i.e., Co–30Cr) and molybdenum-added cobalt-chromium metal alloy (i.e., Co–30Cr–1Mo, Co–30Cr–2Mo, Co–30Cr–3Mo, and Co–30Cr–4Mo) in a steady -state condition with varying sliding velocity and normal load is shown in Figs. 10 and 11. Figure 12 shows the surface morphology of molybdenum-added alloys at different test conditions for L_{25} Taguchi experimental design (Table 3).

Figure 10a shows the wear surface of the molybdenum-free metal alloy where the attendance of molybdenum particles becomes negligible. The surface shows the homogenous in nature due to the absence of molybdenum content as well as ploughing free surfaces. Therefore, the attendance of different micro cracks, shallow grooves, and such kinds of dilemma may be fewer. In Fig. 10b, micro ploughing in the form of parallel and continuous nature along the sliding direction is found due to the attendance of Mo (i.e. 1 wt%) content in the metal alloy and due to which the improper bonding in between the particles was not so strong, and so the material was removed from surfaces during the sliding wear process. Figure 10c shows 2 wt% of molybdenum-added cobalt base metal alloy at 0.78 m/s sliding velocity at constant normal load: 15 N and sliding distance: 1500 m at room temperature. An increase in sliding velocity the upper surface protective layer of the molybdenum reinforced particles can no longer remain stable and the volumetric wear loss is increased due to poor bonding between the hard molybdenum particles and metal–metal alloy (see steady state Fig. 7a) and there may be chances of formation of delamination wear [31] in the subsurface of the worn area which leads to removal of matrix material (see Fig. 10c) from the metal surface during the rubbing process. The materials are removed at the surface of the matrix material in the form of flank-type debris [32]. Figure 10d shows the effect of sliding velocity in steady-state conditions at constant normal load: 15 N and sliding distance: 1500 m, respectively, for 3 wt% of molybdenum-added metal alloy. It is clearly seen in Fig. 10d that the volumetric wear is increased (see Fig. 6d) causes which a massive number of wear strips are formed which are clearly visible on the surface of the prepared metal alloy. However, under similar operating conditions with the increased in molybdenum content (i.e. 4 wt%) in the Co–30Cr alloy, the wear loss drastically reduced (see Fig. 6e) as the hard molybdenum particles act as a protective surface, as shown in Fig. 10e. Similarly, atomic force microscope analysis (AFM) is carried out for worn surfaces of molybdenum-added Co–30Cr-based metal alloys to check the roughness peeks for different wt% of molybdenum content that shown in Fig. 13a–e.

Figure 11 shows the effect of normal load on the volumetric wear of the molybdenum-free and molybdenum-added Co–30Cr metal alloy at a constant sliding velocity: 0.785 m/s and sliding distance: 1500 m, respectively. Figure 11a shows the micrograph of molybdenum-free (i.e., Co–30Cr) metal alloy at low load, i.e., 5 N. At lower loading conditions, the molybdenum-free metal alloy shows commonly delamination wear that confirms the presence of worn surfaces and crack initiation/propagation. However, with the increased in normal load from 5 to 25 N

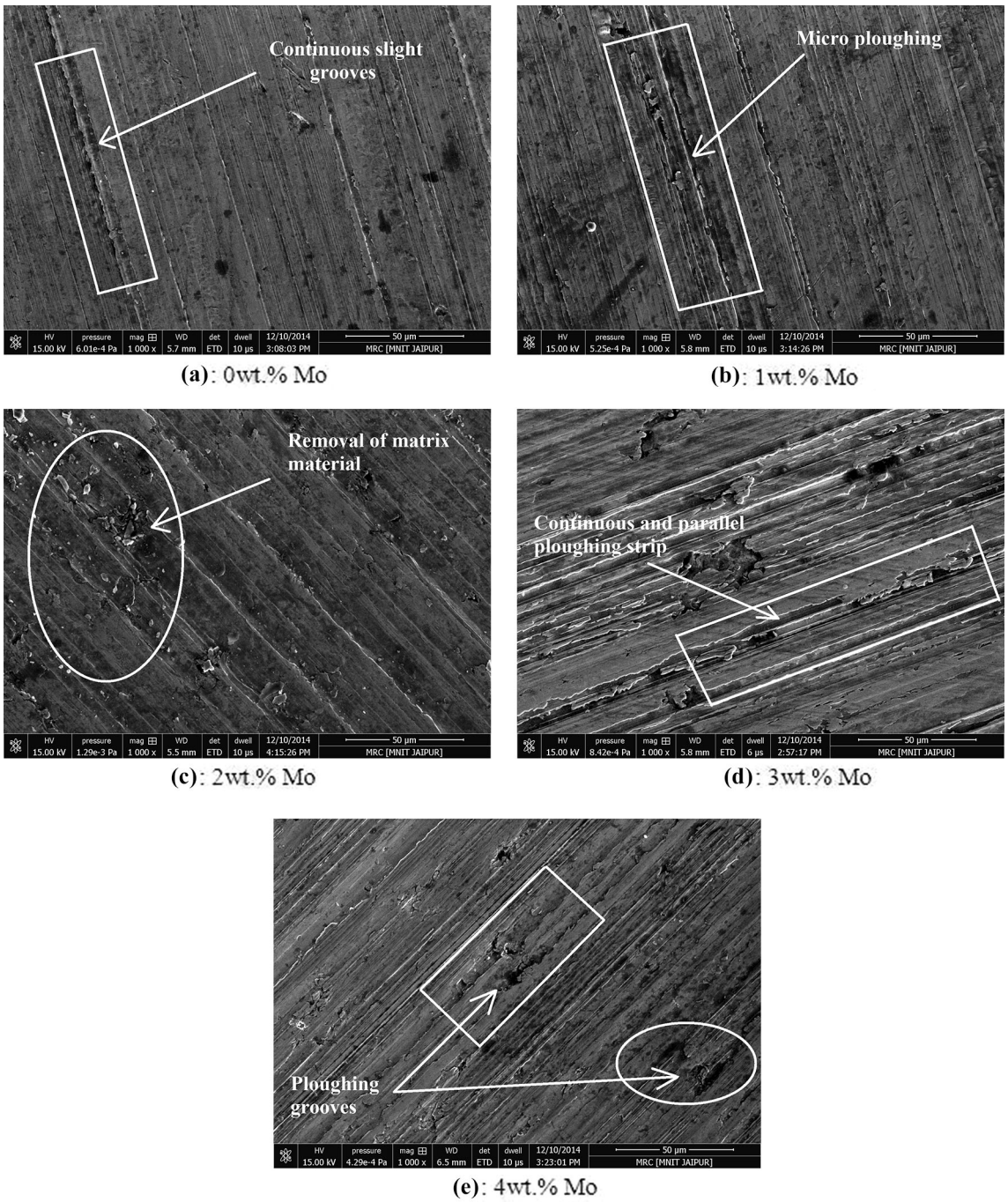

Fig. 10 SEM micrograph of molybdenum (different wt%) added alloys under steady state condition with varying sliding velocity

for the similar molybdenum-free metal alloy, the wear loss significantly increases at a constant sliding velocity: 0.785 m/s and sliding distance: 1500 m, respectively. As compared to Fig. 11a, the breakage area is quite enlarged and the locally damaged matrix material reaches to breaking the surface. Figure 11b shows the wear loss of 1 wt% of molybdenum-added metal alloy (i.e., Co–30Cr–1Mo) at low and high loading condition by keeping the other parameters remaining constant. It is observed that at the low normal load condition the surface micrograph shows removing of surface matrix materials and microcracks to get nearer to the surface with the increased in shear strain thus that causes at the higher load excessive wear. Figure 11c shows 2 wt% of molybdenum-added metal alloy at 10 N load at a constant sliding velocity: 0.785 m/s and sliding distance: 1500 m respectively. An increase in load along the rubbing surface the volumetric wear loss starts increasing and wear track becomes larger. The

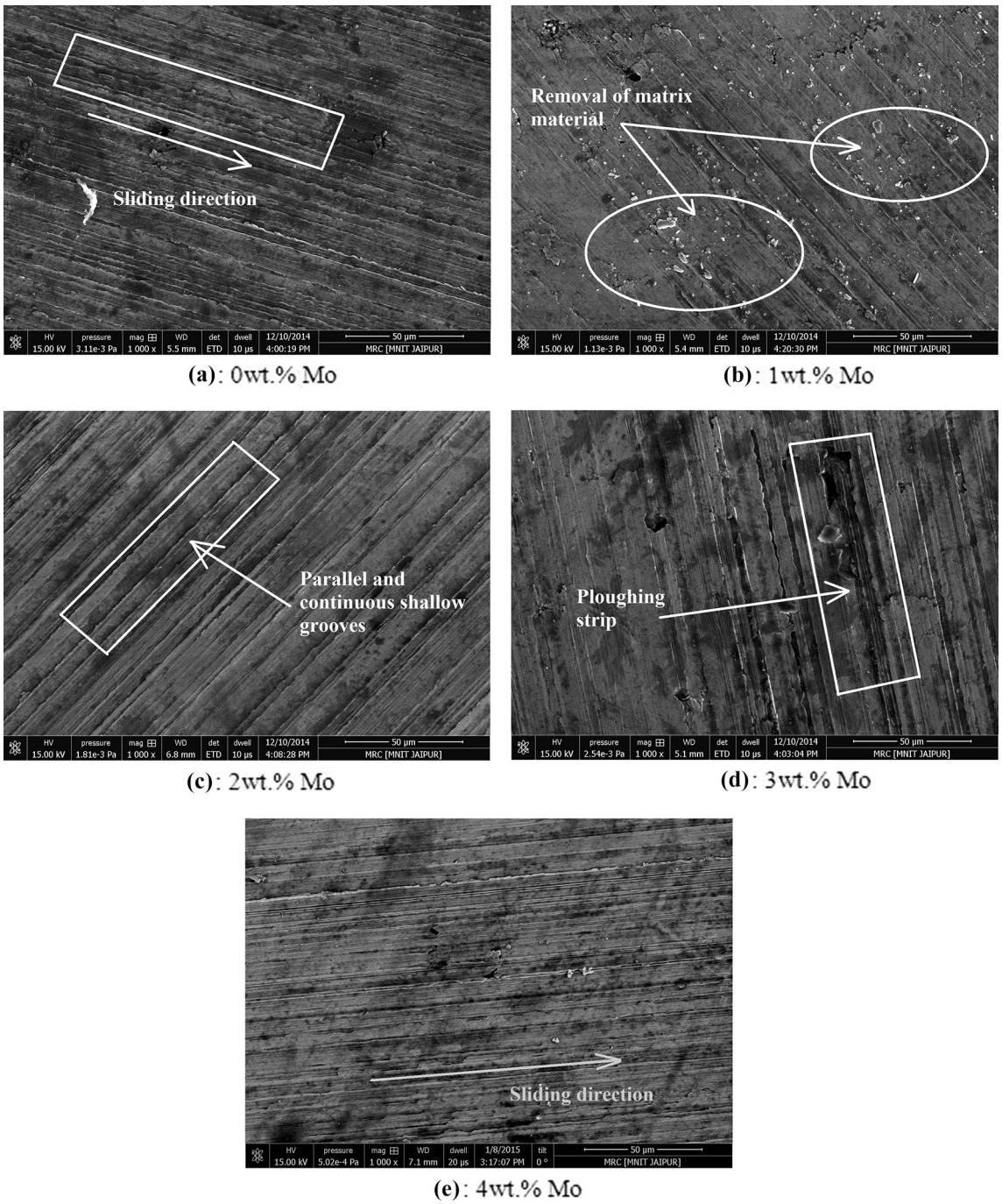

Fig. 11 SEM micrograph of molybdenum (different wt%) added alloys under steady state condition with varying normal load

increased in wear track changes the wear pattern and formed shallow grooves due to less uniform distribution in the matrix material. Similarly, under similar operating conditions, the microstructure wear mechanism shows continuous wear strips (see Fig. 11d) on wear track and the matrix material removed from the surface is in the form of flank-type debris and causes gradually increased in volumetric wear loss (see Fig. 7d). However, on further increased in molybdenum content from 3 to 4 wt% in the Co–30Cr metal alloy, the wear loss is drastically reduced as shown in Fig. 7e and micrograph (Fig. 11e). The reduction is to the presence of hard molybdenum particulates in the matrix and forms a good-quality transfer film that adheres nicely to the rubbing surfaces (see steady state Fig. 7a and morphology Fig. 11e).

Figure 12a–e shows the typical SEM micrographs of the worn surface of the molybdenum-added metal alloy under different operating conditions (Taguchi design of

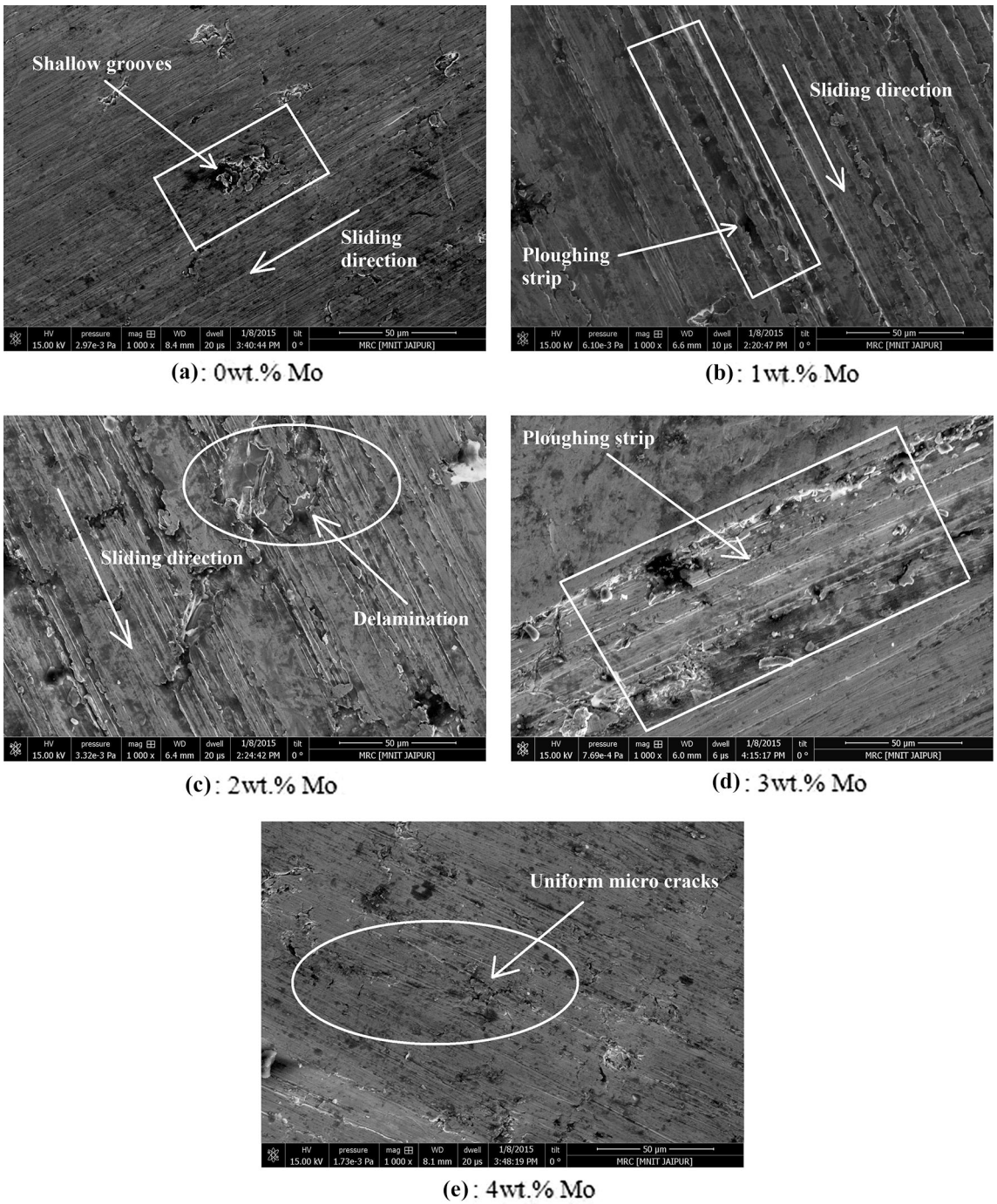

Fig. 12 SEM micrograph of molybdenum (different wt%) added alloys (Taguchi design of experiment)

experiment test run). The matrix materials strongly follow the interaction in between the molybdenum particles and matrix (i.e., Co–30Cr), and this follows the performance of different properties of metal alloy materials for countless applications. The sliding wear test is executed on pin-on-disc tribometer to get the wear mechanism of matrix material with varying operating conditions with time. During wear when two surfaces are in contact that generated a deformation regarding wear debris, ploughing, surface roughness, and many more which directly and indirectly affect the performance of matrix materials. Figure 12a shows the surface microstructure for molybdenum-free (i.e., Co–30Cr) alloy in which the presence of micro ploughing along the sliding direction due to continuous contact of two surfaces during running (See Table 4, Expt. Run 1). However, an increase in sliding velocity from 0.26 to 0.523 m/s under similar loading condition (i.e., 5 N) for addition of 1 wt% Mo in the Co–30Cr metal alloy; the wear

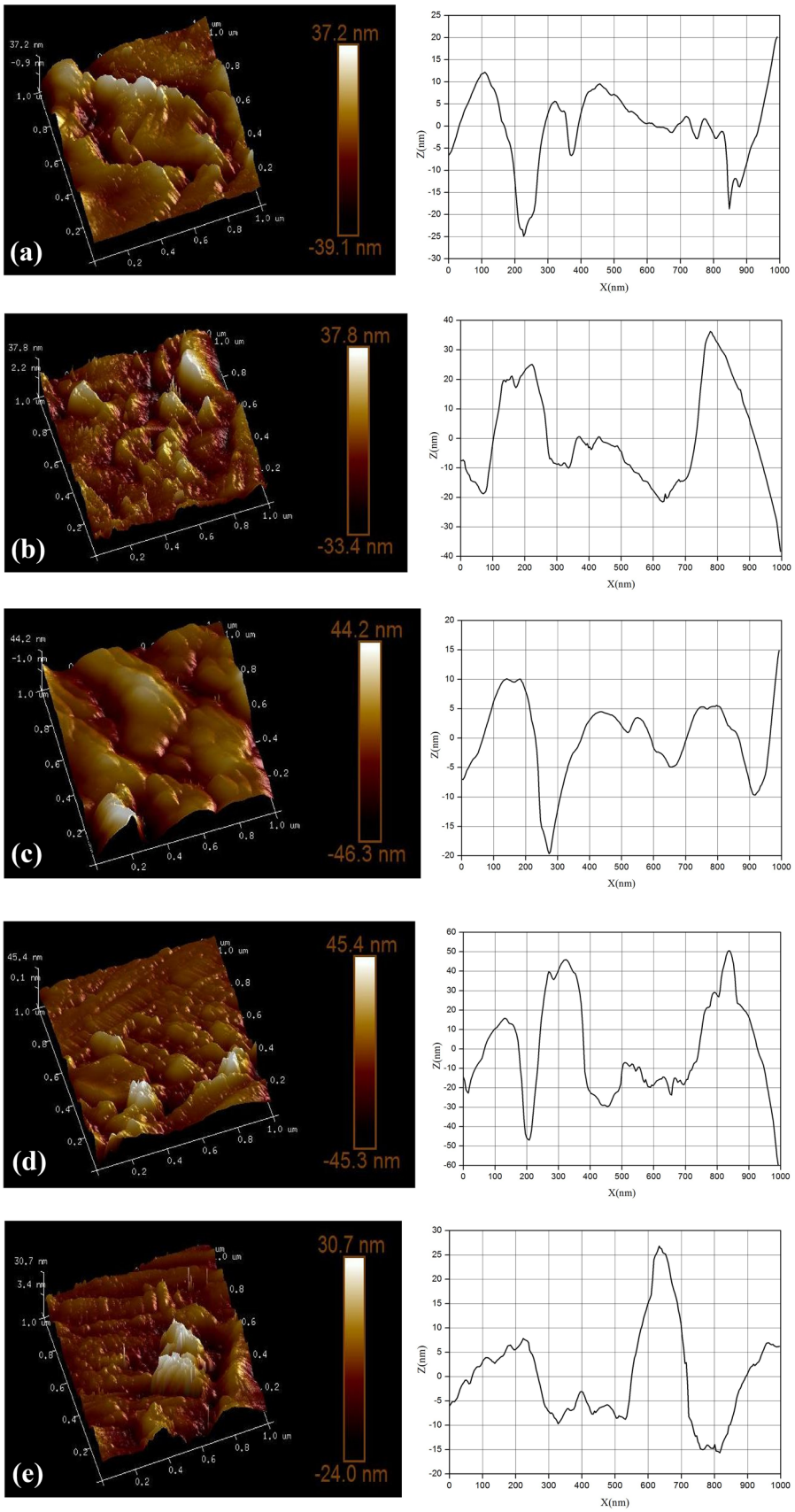

Fig. 13 The 3D AFM micrographs and the line profiles of the molybdenum added alloys **a** 0 wt% Mo, **b** 1 wt% Mo, **c** 2 wt% Mo, **d** 3 wt% Mo, **e** 4 wt% Mo

surfaces show the formation of the parallel and continuous deep ploughing abrasion grooves of the damaged regions, as shown in Fig. 12b (see Table 4, Expt. Run 2). This may be occurring due to the increase in sliding distance and sliding velocity. Similarly, the corresponding AFM micrographs show (Fig. 13b) that the height of sharp tips is also slightly increased, i.e., 37.8 nm.

For 2 wt% Mo particulate added alloy under similar sliding distance (1000 m) with higher normal load (10 N), the micrograph clearly shows that delamination wear occurs and abrasion grooves on the wear surface and causes severe damage as viewed in Fig. 12c (see Table 4, Expt. Run. 6). However, on further increase in normal load (15 N) along with sliding velocity (1.04 m/s) and similar sliding distance (1000 m), the micrograph shows that parallel and continuous deeper ploughing strips with grooves are observed in Fig. 12d (see Table 3, Expt. Run. 15). When the pin and disc surfaces are rubbed together during the sliding wear process at 1.04 m/s sliding velocity, heat is generated at the counterface; and therefore, the molybdenum hard particles loosen from the matrix material. The deeper ploughing phenomenon [33] at that position of the composite material could be the reason for the maximum volumetric wear loss. Figure 12e (see Table 4, Expt. Run. 22) reveals the micrograph of the worn surfaces at maximum normal load (25 N) and sliding velocity (0.523 m/s) for 4 wt% Mo-added biomedical alloy. This shows the least wear loss for 4 wt% of molybdenum-added alloy. As shown in Fig. 12e, very little microcracks are formed uniformly as compared to rest wt% of Mo-added Co–30Cr metal alloys. This may be due to addition of hard molybdenum particulates in the cobalt-chromium (Co–30Cr) alloy.

3.5 Confirmation test

The last step in any design of the experimental approach is to conduct the confirmation test. The purpose of the confirmation test is to validate the conclusions drawn during the analysis phase. The confirmation test is performed by conducting a new set of factor settings $A_3B_4C_1D_2$ and $A_2B_4C_3D_1$to predict the wear volume and friction coefficient, respectively. The estimated S/N ratio for wear volumes and friction coefficient can be calculated by predictive equations:

$$\hat{\eta}_w = \bar{\eta} + (\bar{A}_3 - \bar{\eta}) + (\bar{B}_4 - \bar{\eta}) + (\bar{C}_1 - \bar{\eta}) + (\bar{D}_2 - \bar{\eta}) \quad (3)$$

$$\hat{\eta}_\mu = \bar{\eta} + (\bar{A}_2 - \bar{\eta}) + (\bar{B}_4 - \bar{\eta}) + (\bar{C}_3 - \bar{\eta}) + (\bar{D}_1 - \bar{\eta}), \quad (4)$$

where $\hat{\eta}_w$: predicted average of wear volume, $\hat{\eta}_\mu$: predicted average of friction coefficient, $\hat{\eta}$: overall experimental average, $\bar{A}_2, \bar{A}_3, \bar{B}_4, \bar{C}_1, \bar{C}_3, \bar{D}_1$ and $\bar{D}_2$ are the mean response for factors at designated level. By combining like terms, the equation reduces to:

$$\hat{\eta}_w = \bar{A}_3 + \bar{B}_4 + \bar{C}_1 + \bar{D}_2 - 3\bar{\eta} \quad (5)$$

$$\hat{\eta}_\mu = \bar{A}_2 + \bar{B}_4 + \bar{C}_3 + \bar{D}_1 - 3\bar{\eta}. \quad (6)$$

(5)

A new combination of factor levels $\bar{A}_3, \bar{B}_4, \bar{C}_1, \bar{D}_2$ and $\bar{A}_2, \bar{B}_4, \bar{C}_3, \bar{D}_1$ are used to predict the wear volume and friction coefficient using prediction equations (Eqs. 4 and 5) and the S/N ratio is found to be -14.9564 and 7.89037 dB, respectively. The resulting model seems to be capable of predicting wear volume and friction coefficient to a reasonable accuracy. An error of 1.2% and 1.79% in the S/N ratio of wear volume and friction coefficient is observed and shown in Table 5. However, the error can be further reduced if the number of runs is enhanced. This validates the development of the mathematical model for predicting the measures of performance based on knowledge of the input parameters.

Table 5 Results of the confirmation experiments for wear volume and friction coefficient

Levels	S/N ratio wear volume $A_3B_4C_1D_2$	S/N ratio friction coefficient $A_2B_4C_3D_1$
Prediction	− 14.9564	7.89037
Experimental	− 15.1408	8.03455
Error (%)	1.2	1.79

4 Conclusions

The main purpose of the current study was to determine the effect of molybdenum on the mechanical behavior and wear properties of Co30Cr alloy prepared using high-temperature induction furnace for orthopedic applications. The following conclusions were drawn:

1. It is evident from this study that the density of the fabricated alloys increases with increase in weight percentage (0, 1, 2, 3, and 4 wt%) of Mo particulates in the matrix material. The hardness was also influenced by the addition of Mo particulates, increasing from 653 to 720 Hv.
2. SEM observation shows that from steady-state wear analysis with respect to normal load and sliding velocity, 4 wt% Mo shows maximum wear resistance than other alloy compositions
3. An AFM measurement provides detailed information of wear surface mechanism and illustrates the profile of wear track with the formation of grooves on the worn

out surface. From the results seen in this study, 4 wt% Mo particulate-filled alloy obtained shallow depth and experiences less friction and wear are observed.

4. The optimal combination of control factors has been determined in the Taguchi experimental analysis and found − 9.777 and 6.670 dB S/N ratios for wear loss and friction coefficient, respectively. To validate the experimental results, confirmation experiment has been conducted. An error of 1.2 and 1.79% in the S/N ratio of wear volume and friction coefficient is observed. However, the percentage of error can be further reduced if the number of tests is increased.
5. In future, this study can be extended to corrosion and biocompatibility assessment under body fluid.

References

1. Aherwar A, Singh A, Patnaik A (2016) Cobalt based alloy: a better choice biomaterial for hip implants. Trends Biomater Artif Organs 30(1):50–55
2. Aherwar A, Patnaik A, Bahraminasab M, Singh A (2017) Preliminary evaluations on development of new materials for hip joint femoral head. J Mater Des Appl. https://doi.org/10.1177/1464420717714495
3. Aherwar A, Singh A, Patnaik A (2016) Current and future biocompatibility aspects of biomaterials for hip prosthesis. J Bioeng 3(1):1–22
4. Ozkomur A, Ucar Y, Ekren O, Shinkai RSA, Teixeira ER (2016) Characterization of the interface between cast-to Co–Cr implant cylinders and cast Co–Cr alloys. J Prosthet Dentist 115(5):592–600
5. Rodrigues WC, Broilo LR, Schaeffer L, Knornschild G, Espinoza FRM (2011) Powder metallurgical processing of Co–28% Cr–6% Mo for dental implants: physical, mechanical and electrochemical properties. Powder Technol 206:233–238
6. Dewidar M, Yoon HC, Lim J (2006) Mechanical properties of metals for biomedical applications using powder metallurgy process: a review. Met Mater Int 12:193–206
7. Qiana B, Saeidia K, Kvetkovab L, Lofajc F, Xiaoa C, Shen Z (2015) Defects-tolerant Co–Cr–Mo dental alloys prepared by selective laser melting. Dent Mater. https://doi.org/10.1016/j.dental.2015.09.003
8. Fuzeng R, Weiwei Z, Kangjie C (2016) Fabrication, tribological and corrosion behaviors of ultra-fine grained Co–28 Cr–6 Mo alloy for biomedical applications. J Mech Behav Biomed Mater 60:139–147
9. Ramsden JJ, Allen DM, Stephenson DJ, Alcock JR, Peggs GN, Fuller G, Goch G (2007) The design and manufacture of biomedical surfaces. CIRP Ann Manuf Technol 56(2):687–711
10. Swaminathan V, Gilbert JL (2012) Fretting corrosion of CoCrMo and Ti6Al4V interfaces. Biomaterials 33(22):5487–5503
11. Zhang L, Xiao J, Zhou K (2012) Sliding wear behaviour of silver–molybdenum disulfide composite. Tribol Trans 55:473–480
12. Abedini M, Ghasemi HM, Nili Ahmadabadi M (2012) Effect of normal load and sliding distance on the wear behavior of NiTi alloy. Tribol Trans 55:677–684
13. Brodner W, Bitzan P, Meisinger V, Kaider A, Gottsauner-Wolf F, Kotz R (2003) Serum cobalt levels after metal-on-metal total hip arthroplast. J Bone Jt Surg Am 85:2168
14. Essner A, Schmidig G (2004) The effect of lubricant composition on in vitro wear testing of polymeric acetabular components. J Biomed Mater Res Part B Appl Biomater 68B:45–52
15. A.S.T.M. G99-95 (2000) Standard test method for wear testing with a pin-on disc apparatus. ASTM International, Annual Book of Standards, West Consho-hocken, PA
16. Aherwar A, Singh A, Patnaik A (2016) Study on mechanical and wear characterization of novel Co30Cr4Mo biomedical alloy with added nickel under dry and wet sliding conditions using Taguchi approach. Proc IMechE Part L J Mater Des Appl. https://doi.org/10.1177/1464420716638112
17. Patnaik A, Satapathy A, Mahapatra SS (2009) Study on erosion response of hybrid composites using Taguchi experimental design. J Eng Mater Technol 131:031011–031016
18. Sahoo R, Jha BB, Sahoo TK (2014) Experimental study on the effect of microstructure on dry sliding wear behavior of titanium alloy using Taguchi experimental design. Tribol Trans 57:216–224
19. Montero-Ocampo C, Juarez R, Salinas-Rodriguez A (2007) Effect of FCC-HCP phase transformation produced by isothermal aging on the corrosion resistance of a Co-27Cr-5Mo-0.05C alloy. Metall Mater Trans A 33:2229–2235
20. Patel B, Inam F, Reece M, Edirisinghe M, Bonfield W, Huang J, Angadji A (2014) A novel route for processing cobalt–chromium–molybdenum orthopaedic alloys. J R Soc Interface 1–5
21. Rosenthal R, Cardoso BR, Bott IS, Paranhos RPR, Carvalho EA (2010) Phase characterization in as-cast F-75 Co–Cr–Mo–C alloy. J Mater Sci 45:4021–4028
22. Patel B, Favaro G, Inam F, Reece Michael J, Angadji A, Bonfield W, Huang J, Edirisinghe M (2012) Cobalt-based orthopaedic alloys: relationship between forming route, microstructure and tribological performance. Mater Sci Eng C 32:1222–1229
23. A.S.T.M. F75 (2014) Standard specification for cobalt-28 chromium-6 molybdenum alloy castings and casting alloy for surgical implants (UNS R30075)1, ASTM International, Annual Book of Standards, West Consho-hocken, PA
24. Nwambu CN, Nnuka EE, Odo JU, Nwoye CI, Nwakpa SO (2014) Effect of molybdenum and cobalt addition on structure and mechanical properties of aluminium—12.5% silicon alloy. J Eng Sci Invent 3(4):20–24
25. Shin JC, Doh JM, Yoon JK, Lee DY, Kim JS (2003) Effect of molybdenum on the microstructure and wear resistance of cobalt-base Stellite hardfacing alloys. Surf Coat Technol 166:117–126
26. Hou QY, He YZ, Zhang QA, Gao JS (2007) Influence of molybdenum on the microstructure and wear resistance of nickel-based alloy coating obtained by plasma transferred arc process. Mater Des 28:1982–1987
27. Savarimuthu AC, Taber HF, Megat I, Shadley JR, Rybicki EF, Cornell WC, Emery WA, Somerville DA, Nuse JD (2001) Sliding wear behavior of tungsten carbide thermal spray coatings for replacement of chromium electroplate in aircraft applications. J Therm Spray Technol 10:502–510
28. Rabinowicz E (1995) Friction and wear of materials, 2nd edn. Wiley, New York, p 165
29. Firkins PJ, Tipper JL, Ingham E, Stone MH, Farrar R, Fisher J (2001) A novel low wearing differential hardness, ceramic-on-metal hip joint prosthesis. J Biomech 34(10):1291–1298
30. Doni Z, Alves AC, Toptan F, Gomes JR, Ramalho A, Buciumeanu M, Palaghian L, Silva FS (2013) Dry sliding and tribocorrosion behavior of hot pressed CoCrMo biomedical alloy as compared with the cast CoCrMo and Ti6Al4V alloys. J Mater Des 52:47–57
31. Alvarez-Veraa M, Juarez-Hernandez A, Gonzalez-Rivera CE, Mercado-Solis RD, Hernandez-Rodrigueza MAL (2013) Biotribological response of Co–Cr alloy with added boron under ball-on-disc tests. Wear 301:243–249

32. Pourzal R, Catelas I, Theissmann R, Kaddick C, Fischer A (2011) Characterization of wear particles generated from CoCrMo alloy under sliding wear conditions. Wear 271:1658–1666

33. Hernandez-Rodriguez MAL, Mercado-Solis RD, Perez-Unzueta AJ, Martinez-Delgado DI, Cantu-Sifuentes M (2005) Wear of cast metal–metal pairs for total replacement hip prostheses. Wear 259:958–963